Dielectric permittivity and magnetoelectric coupling in multiferroic BiFeO3 and (Bi0.95La0.05)FeO3 ceramics

Authors: John Doe", do not include affiliations or titles/degrees]

C.-S. Tu, Y. Ding, W.-C. Yang, T.H. Wang, R.R. Chien, V.H. Schmidt, Y.D. Yao, and K.T. Wu, "Dielectric permittivity and magnetoelectric coupling in multiferroic BiFeO3 and (Bi0.95La0.05)FeO3 ceramics," IEEE Transactions on Magnetics 47, 3343-3346 (2011), doi: 10.1109/TMAG.2011.2148104.

Dielectric Permittivity and Magnetoelectric Coupling in Multiferroic $BiFeO_3$ and $(Bi_{0.95}La_{0.05})FeO_3$ Ceramics

C.-S. Tu[1,2], Y. Ding[1,3], W.-C. Yang[2], T. H. Wang[1], R. R. Chien[4], V. H. Schmidt[4], Y. D. Yao[1], and K. T. Wu[1,2]

[1]Graduate Institute of Applied Science and Engineering, Fu Jen Catholic University, Taipei 242, Taiwan
[2]Department of Physics, Fu Jen Catholic University, Taipei 242, Taiwan
[3]Teaching Center of Natural Sciences, Minghsin University of Science and Technology, Hsinchu 304, Taiwan
[4]Department of Physics, Montana State University, Bozeman, MT 57917 USA

Dielectric permittivity and loss of $BiFeO_3$ (BFO) and 5 mol% lanthanum-substituted BFO [$(Bi_{0.95}La_{0.05})FeO_3$ or BFO-5% La] ceramics have been carried out as functions of temperature and frequency. A frequency-dependent and broad dielectric shoulder and maximum were observed in BFO and BFO-5% La near 600–700 K. These dielectric responses are likely due to the magnetoelectric coupling while the antiferromagnetic–paramagnetic transition takes place near the Néel temperature. As an approximation, a barrier model with intrinsic barriers B (in temperature unit) every lattice constant a and extrinsic barriers $B+\Delta$ every distance d is introduced to describe the low-frequency upturn in dielectric loss in the high-temperature region. Good qualitative fits are obtained for BFO and BFO-5% La. This work suggests that 5 mol% La substitution can enhance dielectric response and considerably reduce electric conductivity.

***Index Terms*—Barrier model, $BiFeO_3$, $(Bi_{0.95}La_{0.05})FeO_3$, dielectric permittivity, magnetoelectric coupling.**

I. Introduction

MULTIFERROIC materials enable a coupling interaction between ferromagnetic (FM) and ferroelectric (FE) parameters, which attracted much attention in recent years. This coupling interaction, called the magnetoelectric effect, can be utilized to develop additional functionalities that induce magnetization using external electric field or FE polarization using external magnetic field. The single phase multiferroic $BiFeO_3$ (BFO) is perhaps the only material that possesses both magnetic and FE properties at and above room temperature. BFO has a relatively high antiferromagnetic (AFM)—paramagnetic (PM) Néel temperature at $T_N = 625$–670 K and FE Curie temperature at $T_C = 1083$–1143 K [1]–[5]. A rhombohedral structure of $R3c$ space group ($a_R = 5.616$ Å and $\alpha_R = 59.35°$) was reported for bulk BFO solution [6], and can also be indexed based on the pseudo-cubic lattice ($a_p = 3.96$ Å) [7]. The neutron powder diffraction suggested that BFO undergoes a first-order phase transition at $T_C \cong 1093$ K from a FE rhombohedral to a paraelectric (PE) orthorhombic $GdFeO_3$-type structure [8], [9].

It has been a challenge to synthesize single-phase BFO ceramics with promising magnetization and FE polarization, because current leakage and second phases can easily occur during the sintering process [10]. Most reported BFO ceramics exhibit a small remanent magnetization and FE polarization [9]–[12]. To enhance FM and FE features, many studies have focused on substituted BFO ceramics with various ion substitutions in the A or B sites of the perovskite structure [13]–[18]. In particular, A-site substitutions of rare-earth cations are expected to suppress the spiral magnetic modulation and thus enhance an FM response [9].

The ionic radii of La^{3+} and Bi^{3+} are almost equivalent. The first phase diagram as a function of La concentration for $Bi_{1-x}La_xFeO_3$ was obtained by Polomska *et al.* [19], [20]. Below 10% La substitution, $Bi_{1-x}La_xFeO_3$ maintains a rhombohedral structure. Structures change to orthorhombic and tetragonal for $Bi_{0.8}La_{0.2}FeO_3$ and $Bi_{0.7}La_{0.3}FeO_3$, respectively [21].

Though BFO and $Bi_{1-x}La_xFeO_3$ have been studied extensively in recent years, their temperature- and frequency-dependent dielectric response and magnetoelectric coupling still lack understanding. The main focus of this work is to develop a 1-D barrier conductivity model to explain the large low-frequency upturn in dielectric loss upon heating. Another aim is to study the La-substitution effect on dielectric response in BFO ceramics.

II. Experimental Procedure

The BFO and BLFO ceramics were prepared by the solid state reaction method. For synthesis of BFO, starting powders of Bi_2O_3 and Fe_2O_3 (purity $\geq 99.0\%$) were weighed in 1:1 ratio and then mixed in an agate mortar for more than 24 h using alcohol as a medium. The mixture was dried before calcining at 1073 K for 3 h. The calcined powder was mixed with polyvinyl acetate as a binder for granulation. The ground mixture was then pressed into a 1.0-cm diameter disk, which was sintered at 1023 K for 1 h. For synthesis of BFO-5% La ceramic, starting powders of Bi_2O_3, La_2O_3, and Fe_2O_3 were weighed in a 0.95:0.05:1 molar ratio. The calcined disk was sintered at 1153 K for 0.5 h. The densities of both ceramics are higher than 90% of the theoretical values.

For structural study, a Rigaku Model MultiFlex X-ray diffractometer was employed. A Wayne-Kerr Analyzer PMA3260A was used to obtain the real (ε') and imaginary (ε'') parts of dielectric permittivity.

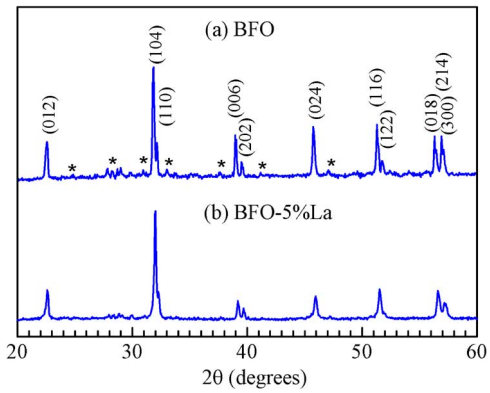

Fig. 1. Room-temperature XRD spectra of (a) BFO and (b) BFO-5% La ceramics. "∗" corresponds to second phases.

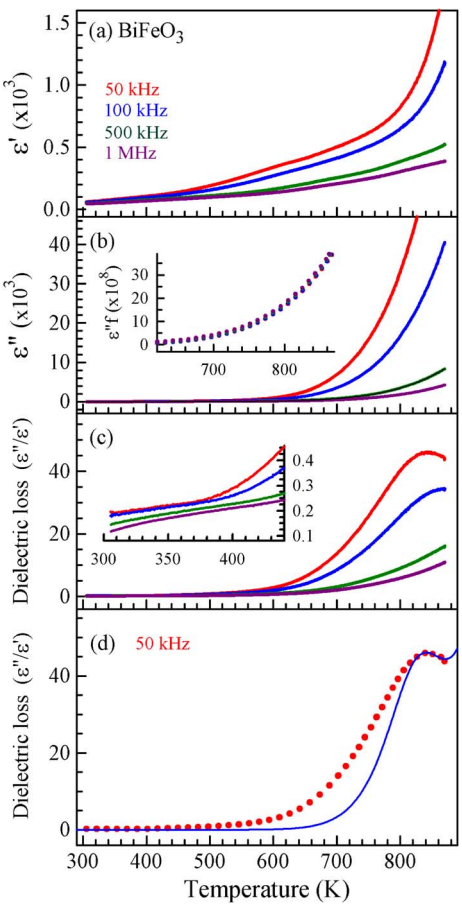

Fig. 2. Frequency-dependent (a) ε', (b)ε'', and (c) dielectric loss for BFO upon heating. (d) Solid line is a fit of barrier model to loss (dotted line) for $f = 50$ kHz with parameters: $\varepsilon'_\infty = 1520$/T, $a = 0.395$ nm, $d = 2$ μm, $B = 13\,800$ K, and $\Delta = 5800$ K.

III. Results and Discussion

Fig. 1 shows room-temperature XRD spectra of BFO and BFO-5% La ceramics. BFO and BFO-5% La show a similar XRD spectrum and have a rhombohedral perovskite structure. Some minor second phases occur in BFO and are possible $Bi_{25}FeO_{39}$ or $Bi_2Fe_4O_9$ as indicated by "∗" [6]. BFO-5% La exhibits less second phase, implying that the A-site La-substitution can stabilize the single-phase perovskite structure.

Figs. 2 and 3 show temperature- and frequency-dependent dielectric permittivities (ε' and ε'') and dielectric loss ($\tan\delta = \varepsilon''/\varepsilon'$) of BFO and BFO-5% La. In BFO-5% La, the dielectric maximum of ε' in the region of 600–700 K exhibits a broad frequency dispersion that shifts to higher temperature as frequency increases. The ε' of BFO exhibits a rather broad shoulder followed by an exponential increase upon heating. The frequency-dependent broad dielectric maximum or shoulder in the region 600–700 K is likely activated by the AFM-PM transition near the Néel temperature (T_N) [22].

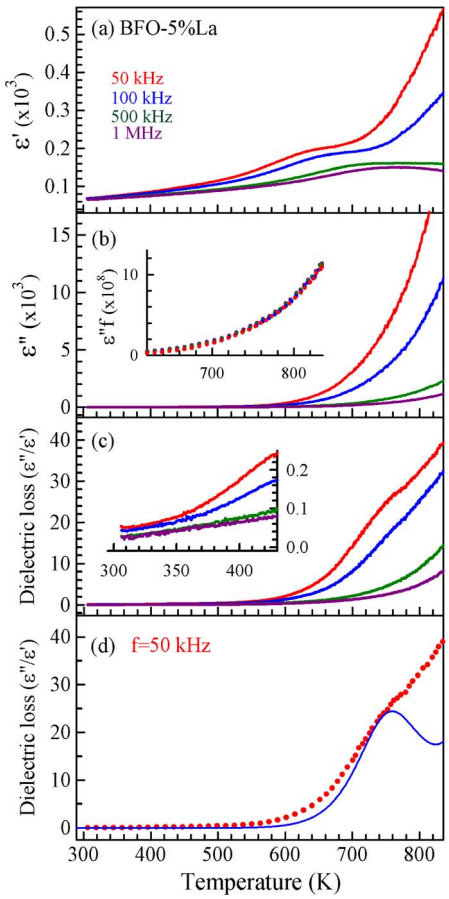

Fig. 3. Frequency-dependent (a) ε', (b)ε'', and (c) dielectric loss for BFO-5% La upon heating. (d) Solid line is a fit of barrier model to loss (dotted line) for $f = 50$ kHz with parameters: $\varepsilon'_\infty = 2300$/T, $a = 0.395$ nm, $d = 2$ μm, $B = 12\,300$ K, and $\Delta = 5800$ K.

The room-temperatures ε' of BFO and BFO-5% La are about 60 and 70, respectively. As shown in the insets of Figs. 2(c) and 3(c), the dielectric losses ($\tan\delta$) of BFO and BFO-5% La ceramics at room temperature are about 0.1–0.2 and 0.02–0.05, respectively, indicating that 5 mol% La substitution can considerably reduce electric loss. BFO and BFO-5% La exhibit an exponential upturn in ε'' upon heating with magnitude proportional to $1/f$. This is illustrated by $\varepsilon'' f$ plots which almost superimpose in the same upturn curves above 600 K for different frequencies in the insets of Figs. 2(b) and 3(b). A broad maximum or shoulder appears in the low-frequency dielectric loss above 700 K in Figs. 2(c) and 3(c). These high-temperature dielectric responses indicate the phase-shifted hopping conductivity associated with a barrier distribution [23].

As an attempt to understand the low-frequency and high-temperature dielectric anomalies, a 1-D barrier model was derived in the Section IV.

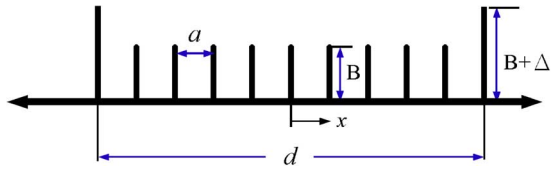

Fig. 4. One-dimensional barrier model with intrinsic barriers B at spacing a, and extrinsic barriers $B+\Delta$ at spacing d.

IV. 1-D Barrier Model

Fig. 4 is an illustration of a 1-D barrier model, in which B represents the intrinsic barriers spaced a distance a apart, where a is of the order of a lattice constant. $B+\Delta$ are extrinsic barriers spaced a distance d apart, where d could be of the order of grain size in the ceramic matrix.

The attempt frequency for crossing the barriers is $\nu = k\Theta/h$, where k, Θ, and h are the Boltzmann constant, Debye temperature, and Planck's constant. The complex ac conductivity $\sigma(\omega,T) = \sigma' + i\sigma''$ can be defined as

$$\sigma(\omega,T) = (J + \partial D/\partial t)/\langle E\rangle. \tag{1}$$

J and $\partial D/\partial t$ are conduction current density and the displacement current density. $\langle E\rangle$ is the spatially averaged measured field, whereas E is position dependent. The complex dielectric permittivity $\varepsilon(\omega,T) = \varepsilon' - i\varepsilon''$ is related to ac conductivity by

$$\varepsilon' = \sigma''/\varepsilon_o\omega \quad \varepsilon'' = \sigma'/\varepsilon_o\omega \tag{2}$$

where ε_o is the MKS constant 8.854×10^{-12} C^2/Nm^2. For high-frequency conductivity, we assume conductivity with a temperature-independent carrier density n and carrier charge q. The high-frequency conductivity $\sigma_\infty = J/E$, taking into account that the number of carrier per unit area in a unit-cell layer on either side of a barrier layer is na and their attempt frequency for crossing the barrier is ν, can be expressed by

$$\begin{aligned}\sigma_\infty &= q\nu na\left\{e^{\left(-kB+\frac{1}{2}qEa\right)/kT} - e^{\left(-kB-\frac{1}{2}qEa\right)/kT}\right\}/E \\ &\cong (q^2\nu na^2/kT)e^{-B/T} = (nq^2a^2\Theta/hT)e^{-B/T}.\end{aligned} \tag{3}$$

Using the Gauss law $\partial D/\partial x = \rho$ and the diffusion equation $\partial\rho/\partial t = \overline{D}\nabla^2\rho$, (1) becomes

$$\begin{aligned}J &= \sigma_\infty E - \overline{D}\partial\rho/\partial x = \sigma_\infty E - \mu kT(\partial\rho/\partial x)/q \\ &= \sigma_\infty E - \sigma_\infty\tau(\partial\rho/\partial x).\end{aligned} \tag{4}$$

$\overline{D}$ and ρ are diffusion coefficient and charge density. The Einstein relation $q\overline{D} = \mu kT = (v_d/E)kT$, $\tau = kT/(nq^2)$, and $\sigma_\infty = nq\mu = nq(v_d/E)$ were used in (4). $\nu_{\rm d}$ is the drift velocity. Taking the x derivative of (4), we have

$$\partial E/\partial x = (\partial J/\partial x)/\sigma_\infty + \tau(\partial^2\rho/\partial x^2). \tag{5}$$

To eliminate J and E, the 1-D Gauss's law $\partial E/\partial x = \rho/\varepsilon_\infty$ and continuity equation $\partial J/\partial x = -\partial\rho/\partial t$ were used in (5), i.e.,

$$\partial^2\rho/\partial x^2 - \rho/(\tau\varepsilon_\infty) - (\partial\rho/\partial t)/(\tau\sigma_\infty) = 0. \tag{6}$$

This equation is separable, and we may assume

$$\rho(x,t) = f(x)e^{i\omega t} \tag{7}$$

for which the $f(x)$ equation becomes

$$(\partial^2 f/\partial x^2) - \alpha^2 f = 0 \text{ and } \alpha^2 = 1/(\tau\varepsilon_\infty) + i\omega/(\tau\sigma_\infty). \tag{8}$$

The solution for $f(x)$ is

$$\begin{aligned}f(x) &= Ae^{\alpha x} + Be^{-\alpha x} \\ \alpha &= \left[\left(\frac{1}{\tau\varepsilon_\infty}\right)^2 + \left(\frac{\omega}{\tau\sigma_\infty}\right)^2\right]^{1/4} \\ &\quad\times e^{(i/2)\tan^{-1}(\omega\varepsilon_\infty/\sigma_\infty)}.\end{aligned} \tag{9}$$

For a neutral material, $\rho\,(x=0) = 0$ at the midpoint between higher harriers is expected, so $B = -A$. Then, (7) becomes

$$\rho(x,t) = A'\sinh(\alpha x)e^{i\omega t}. \tag{10}$$

From here on, the time dependence e^{iwt} will be omitted in expressions for ρ, J, and E. We next need to find expressions for the total current J_t and for the average field $\langle E\rangle$. Since J_t is position independent, we choose to calculate J and $\partial D/\partial t$ at the high barriers. From (4), the current density J at $x = d/2$ can be expressed by

$$J(d/2) = \sigma_\infty\left[E(d/2) - \tau(\partial\rho/\partial x)\right]e^{-\Delta/T}. \tag{11}$$

The difference in carrier density across the higher barriers is

$$\rho(d/2) - \rho(-d/2) = 2\rho(d/2) \quad \partial\rho/\partial x \cong 2\rho(d/2)/a. \tag{12}$$

Thus

$$\begin{aligned}J(\pm d/2) &= \sigma_\infty\left\{E(\pm d/2) - \tau\left[\rho(-d/2) - \rho(d/2)\right]/a\right\}e^{-\Delta/T} \\ &= \sigma_\infty e^{-\Delta/T}\left\{E(\pm d/2) + 2\tau a^{-1}A'\sinh(b)\right\}\end{aligned} \tag{13}$$

where $b = \alpha d/2$. Using (4) and $\partial\rho/\partial x = A'\alpha\cosh(\alpha x)$, we obtain

$$\begin{aligned}E(\pm d/2) = \tau A'\left[2a^{-1}e^{-\Delta/T}\sinh(b) + \alpha\cosh(b)\right] \\ \times(1 - e^{-\Delta/T})^{-1}.\end{aligned} \tag{14}$$

Then, (13) becomes

$$\begin{aligned}J(\pm d/2) = \sigma_\infty\tau A'e^{-\Delta/T}\left[\alpha\cosh(b) + 2a^{-1}\sinh(b)\right] \\ \times(1 - e^{-\Delta/T})^{-1}.\end{aligned} \tag{15}$$

From (14) and (15), we can determine the total current

$$\begin{aligned}J_t(t) &= J + \partial D/\partial t = J + i\omega\varepsilon_\infty E \\ &= e^{i\omega t}\tau A'e^{-\Delta/T} \\ &\quad\times\left\{\sigma_\infty\left[\alpha\cosh(b) + 2a^{-1}\sinh(b)\right]\right. \\ &\qquad\left.+i\omega\varepsilon_\infty\left[2a^{-1}\sinh(b) + e^{\Delta/T}\alpha\cosh(b)\right]\right\} \\ &\quad\times(1 - e^{-\Delta/T})^{-1}.\end{aligned} \tag{16}$$

$$\varepsilon' = \varepsilon'_\infty \left\{ \frac{(b+2r-b^2-br+be^{\Delta/T})\cos^2\phi(e^{\Delta/T}-1)+(br+b^2e^{\Delta/T})\sin^2\phi e^{\Delta/T}}{DEN} + \frac{(r/b+e^{\Delta/T})(b^2\cos^2\phi+br)}{DEN} \right\}$$

$$\varepsilon'' = \frac{\sigma_\infty}{\omega\varepsilon_o} \left\{ \frac{(b+r)\left[r+b\sin^2\phi e^{\Delta/T}+\cos^2\phi(e^{\Delta/T}-1+b)\right]}{DEN} + \frac{\left(\omega^2\varepsilon_\infty^2/\sigma_\infty^2\right)(r+be^{\Delta/T})\cos^2\phi(e^{\Delta/T}-1)(b-1)}{DEN} \right\}$$

$$DEN = \left[r+b\sin^2\phi e^{\Delta/T}+\cos^2\phi(e^{\Delta/T}+b-1)\right]^2 + \left[\cos^2\phi(e^{\Delta/T}-1)(b-1)\omega\varepsilon_\infty/\sigma_\infty\right]^2 \quad (18)$$

The electric field E in the interval $-d/2 < x < d/2$ can be obtained by

$$E(x) = \int \rho(x)dx/\varepsilon_\infty = E(-d/2)+(A'/\varepsilon_\infty)\int_{-d/2}^{x}\sinh(\alpha x)dx.$$

Then, the average field $\langle E\rangle$ can be calculated by

$$\langle E\rangle = E(-d/2)+\frac{1}{d}\int_{-d/2}^{d/2}(A'/\alpha\varepsilon_\infty)\cosh(\alpha x)dx. \quad (17)$$

By using (1), (2), (16), and (17) and carrying considerable algebraic calculation, we obtain (18) shown at the top of the page, where $r = d/a$, $b = \alpha d/2$, $\varepsilon_\infty = \varepsilon_o\varepsilon'_\infty$, and $\phi = \tan^{-1}(\omega\varepsilon_\infty/\sigma_\infty)$.

In this calculation, we chose $\Theta = 300$ K and assumed that ε_∞ obeys the Curie–Weiss law, $\varepsilon_\infty = \varepsilon_o \mathrm{C/T}$. Based on XRD and SEM results, we chose the lattice constant of $a = 0.395$ nm and extrinsic barrier distance of $d = 2$ μm. The solid lines in Figs. 2(d) and 3(d) are fits of the barrier model to the upturn dielectric loss $(\tan\delta = \varepsilon''/\varepsilon')$ from $f = 50$ kHz for BFO and BFO-5% La ceramics. From the fits, the intrinsic barrier heights B of BFO and BFO-5% La are 13 800 K ($\sim$1.19 eV) and 12 300 K ($\sim$1.06 eV), respectively. The discrepancy between the barrier-model fits and experimental data could be due to other conductivity contributions, such as having both ionic and electronic conductivity, and to actual higher barriers having a distribution of spacings d and heights $B+\Delta$. The larger discrepancy below 750 K in BFO may imply that the electronic conductivity contributes more in BFO than in BFO-5% La.

V. Conclusion

A frequency-dependent and broad shoulder and dielectric maximum occur near 600 and 700 K, respectively, in BFO and BFO-5% La ceramics and are likely triggered by the magnetoelectric coupling where the AFM-PM transition proceeds near the Néel temperature of 625–670 K. A 1-D barrier model can qualitatively fit the large low-frequency upturn in dielectric loss upon heating. The 5 mol% La substitution can enhance dielectric response and considerably reduce electric conductivity.

Acknowledgment

This work was supported by the National Science Council of Taiwan Grant 97-2112-M-030-003-MY3.

References

[1] J. R. Teague, R. Gerson, and W. J. James, *Solid State Commun.*, vol. 8, p. 1073, 1970.
[2] P. Fischer, M. Polomska, I. Sosnowska, and M. Szymański, *J. Phys. C*, vol. 13, p. 1931, 1980.
[3] M. M. Kumar and V. R. Palkar, *Appl. Phys. Lett.*, vol. 76, p. 2764, 2000.
[4] J.-C. Chen and J.-M. Wu, *Appl. Phys. Lett.*, vol. 91, p. 182903, 2007.
[5] B. Ramachandran and M. S. R. Rao, *Appl. Phys. Lett.*, vol. 95, p. 142505, 2009.
[6] F. Kubel and H. Schmid, *Acta Crystallogr., Sect. B: Structure Science*, vol. 46, p. 698, 1990.
[7] Y. Yang, V. G. M. Annamdas, C. Wang, and Y. Zhou, *Sensors*, vol. 8, p. 271, 2008.
[8] D. C. Arnold, K. S. Knight, F. D. Morrison, and P. Lightfoot, *Phys. Rev. Lett.*, vol. 102, p. 027602, 2009.
[9] I. Levin, S. Karimi, V. Provenzano, C. L. Dennis, H. Wu, T. P. Comyn, T. J. Stevenson, R. I. Smith, and I. M. Reaney, *Phys. Rev. B*, vol. 81, p. 020103(R), 2010.
[10] R. Palai, R. S. Katiyar, H. Schmid, P. Tissot, S. J. Clark, J. Robertson, S. A. T. Redfern, G. Catalan, and J. F. Scott, *Phys. Rev. B*, vol. 77, p. 014110, 2008.
[11] Y. P. Wang, L. Zhou, M. F. Zhang, X. Y. Chen, J. M. Liu, and Z. G. Liu, *Appl. Phys. Lett.*, vol. 84, p. 1731, 2004.
[12] S. T. Zhang, M. H. Lu, D. Wu, Y. F. Chen, and N. B. Ming, *Appl. Phys. Lett.*, vol. 87, p. 262907, 2005.
[13] G. L. Yuan and S. W. Or, *Appl. Phys. Lett.*, vol. 88, p. 062905, 2006.
[14] K. Sigh, R. K. Kotnala, and M. Singh, *Appl. Phys. Lett.*, vol. 93, p. 212902, 2008.
[15] A. Singh, V. Pandey, R. K. Kotnala, and D. Pandey, *Phys. Rev. Lett.*, vol. 101, p. 247602, 2008.
[16] G. L. Yuan, S. W. Or, J. M. Liu, and Z. G. Liu, *Appl. Phys. Lett.*, vol. 89, p. 052905, 2006.
[17] S. Karimi, I. M. Reaney, I. Levin, and I. Sterianou, *Appl. Phys. Lett.*, vol. 94, p. 112903, 2009.
[18] P. Pandit, S. Satapathy, P. K. Gupta, and V. G. Sathe, *J. Appl. Phys.*, vol. 106, p. 114105, 2009.
[19] M. Polomska, W. Kaczmarek, and Z. Pajak, *Phys. Stat. Sol.*, vol. 23, p. 567, 1974.
[20] M. Polomska and W. Kaczmarek, *Acta Phys. Polonica A*, vol. 45, p. 199, 1974.
[21] Z. X. Cheng, A. H. Li, X. L. Wang, S. X. Dou, K. Ozawa, H. Kimura, S. J. Zhang, and T. R. Shrout, *J. Appl. Phys.*, vol. 103, p. 07E507, 2008.
[22] T.-H. Wang, C.-S. Tu, H.-Y. Chen, Y. Ding, T. C. Lin, Y.-D. Yao, V. H. Schmidt, and K.-T. Wu, *J. Appl. Phys.*, vol. 109, p. 044101, 2011.
[23] V. H. Schmidt, G. F. Tuthill, C.-S. Tu, T. V. Schogoleva, and S. C. Meschia, *J. Phys. Chem. Solid*, vol. 57, p. 1493, 1996.